Species-selective lattice launch for precision atom interferometry

2015 New J. Phys. 17 123002

(http://iopscience.iop.org/1367-2630/17/12/123002)

New Journal of Physics
The open access journal at the forefront of physics

Deutsche Physikalische Gesellschaft DPG
IOP Institute of Physics

Published in partnership with: Deutsche Physikalische Gesellschaft and the Institute of Physics

OPEN ACCESS

RECEIVED
22 July 2015

REVISED
26 October 2015

ACCEPTED FOR PUBLICATION
27 October 2015

PUBLISHED
4 December 2015

PAPER

Species-selective lattice launch for precision atom interferometry

R Chamakhi[1,2], H Ahlers[3], M Telmini[1], C Schubert[3], E M Rasel[3] and N Gaaloul[3]

[1] LSAMA Department of Physics, Faculty of Sciences of Tunis, University of Tunis-El Manar, 2092 Tunis, Tunisia
[2] National Centre for Nuclear Sciences and Technology, 2020 Sidi Thabet Technopark, Tunisia
[3] Institute of Quantum Optics, Leibniz University of Hanover, Welfengarten 1, D-30167 Hanover, Germany

E-mail: gaaloul@iqo.uni-hannover.de

Keywords: atom interferometry, equivalence principle, atomic fountains, cold atoms, Bose–Einstein condensates, optical lattices

Abstract

Long-baseline precision tests based on atom interferometry require drastic control over the initial external degrees of freedom of atomic ensembles to reduce systematic effects. The use of optical lattices (OLs) is a highly accurate method to manipulate atomic states in position and momentum allowing excellent control of the launch in atomic fountains. The simultaneous lattice launch of two atomic species, as required in a quantum test of the equivalence principle, is however problematic due to crosstalk effects. In this article, we propose to selectively address two species of alkalines by applying two OLs at or close to *magic-zero* wavelengths of the atoms. The proposed scheme applies in general for a pair of species with a vastly different ac Stark shift to a laser wavelength. We illustrate the principle by studying a fountain launch of condensed ensembles of ^{87}Rb and ^{41}K initially co-located. Numerical simulations confirm the fidelity of our scheme up to few nm and nm s^{-1} in inter-species differential position and velocity, respectively. This result is a pre-requisite for the next performance level in precision tests.

1. Introduction and motivations

Manipulating cold atomic ensembles with optical dipole traps is an exquisite tool to address their external degrees of freedom [1]. The Stark effect resulting from these beams realizes so-called optical tweezers and allows to precisely confine or move cold atoms or Bose–Einstein condensates (BEC) [2, 3] and prepare them in desired position and momentum states. Interference of counter-propagating dipole beams creates a conservative periodic potential known as an optical lattice (OL) [4]. Atoms trapped at the potential minima of this periodic structure realize solid state physics-like systems with an unprecedented possibility to control the lattice properties. If the two interfering beams are relatively detuned, the lattice can displace the atoms. If the detuning is time-dependent, it accelerates them via Bloch oscillations [5, 6] in analogy with electrons in a solid subject to an electric field. This method is very efficient in transferring large and quantized momenta to the atoms [7] putting them in well defined momentum states. Therefore, it is extensively used in precision atom interferometry [8–12].

The free evolution of an atomic ensemble in the gravitational field interrogated in a Mach–Zehnder light-pulse interferometer realizes a measurement of the gravitational acceleration g [13–17]. When two atomic ensembles of different masses are dropped in the gravity field, a comparison of their accelerations realizes a universality of free fall test or test of the weak Einstein's equivalence principle (WEP) [18]. Since violations of this principle are predicted at different levels in competing theories to unify fundamental interactions [19], such an experimental test can have a major impact in (in)validating these models. In recent years, atom interferometers performed WEP tests up to 10^{-7} in the Eötvös ratio [20–23] parametrized by η

$$\eta = \frac{\left(a_1 - a_2\right)}{\left(a_1 + a_2\right)/2} = \frac{\delta a}{\bar{a}}, \tag{1}$$

where a_1 and a_2 are the accelerations experienced by the test masses 1 and 2, respectively, $\delta a = (a_1 - a_2)$ and $\bar{a} = (a_1 + a_2)/2$. Since the sensitivity of an atom interferometer typically scales quadratically with the pulse separation time T, there is an obvious incentive for using atomic fountains on ground to augment the available experimental time. This geometry is at the heart of recent proposals expected to open a new era of precision WEP tests (up to seven orders of magnitude expected improvement over state-of-the-art) by performing it in 10 m tall towers [24–26]. The idea is to launch two atomic ensembles of different atomic species using accelerated lattices before operating two simultaneous Mach–Zehnder atom interferometers, thus comparing the local gravity acceleration experienced by each.

In such a test performed in the vertical direction z, the differential velocity δv_z between the two species at the end of the acceleration stage couples e.g. to local gravity gradients (GG) resulting in a differential acceleration bias δa. In line with recent and proposed experiments, we assume the typical Mach–Zehnder ($\pi/2$-π-$\pi/2$) pulse geometry. The full interferometer time $2T$ shall be the same for both species, but the effective wave numbers k_1 and k_2 may differ. The phase shift due to the GG in each interferometer $i = 1, 2$ is [27]

$$\phi_i = -k_i T_{zz} v_{z,i} T^3, \tag{2}$$

which divided by the scale factor $k_i T^2$ leads to an acceleration equivalent bias of

$$a_i = -T_{zz} v_{z,i} T, \tag{3}$$

for a launch velocity $v_{z,i}$. Thus, the differential acceleration is

$$\delta a = -T_{zz} T \left(v_{z,1} - v_{z,2} \right) = -T_{zz} T \delta v_z, \tag{4}$$

with $\delta v_z = v_{z,1} - v_{z,2}$. T_{zz} denotes the first order GG tensor $\partial_z g_z$. In the considered case, the fountain is solely realized in the z-direction and therefore the other gradient tensor terms can safely be neglected. Phase shifts due to higher order tensors are orders of magnitude smaller than ϕ_i, thus not considered here. Dependent on the vibrational background, an additional mechanical accelerometer might be necessary to recover the interferometer signals of the weak equivalence principle as suggested in [28]. This GG coupling can be eliminated in a particular four-pulse atom interferometer scheme [29] at the cost, however, of a degraded (about a factor 5 lower) sensitivity to the gravity acceleration.

A GG T_{zz} with an uncertainty ΔT_{zz} parallel to the effective wave vectors couples to a differential velocity of the two ensembles δv_z oriented in the same direction with an uncertainty $\Delta \delta v_z$. Since both the GG and the differential velocity are known within their uncertainties, a post-correction reduces the GG contribution to an uncertainty of

$$\Delta \eta = \Delta \delta a / \bar{a} = -T \cdot \left(\left| T_{zz} \Delta \delta v_z \right| + \left| \Delta T_{zz} \delta v_z \right| + \left| \Delta T_{zz} \Delta \delta v_z \right| \right) / \bar{a}. \tag{5}$$

Using compensation masses within the region where the atom interferometer is formed as proposed in [30] would only reduce the contribution of the first term in equation (5) proportional to T_{zz} without relaxing the knowledge level required for ΔT_{zz}.

If one considers the case of Earth's GG on ground $T_{zz} = -3 \times 10^{-6}\ \mathrm{s}^{-2}$, and a differential velocity of $\delta v = 0\ \mu\mathrm{m\ s}^{-1}$ with an uncertainty $\Delta \delta v = \pm 0.2\ \mu\mathrm{m\ s}^{-1}$, one would reach an uncertainty in $\Delta \eta$ of 10^{-13} even with a modest knowledge of the GG of $\Delta T_{zz} = 3 \times 10^{-6}\ \mathrm{s}^{-2}$. If $\delta v_z = 100\ \mu\mathrm{m\ s}^{-1}$ and $\Delta \delta v = \pm 0.2\ \mu\mathrm{m\ s}^{-1}$, then a characterization of T_{zz} to 0.2% corresponding to $\Delta T_{zz} = 6 \times 10^{-9}\ \mathrm{s}^{-2}$ would be necessary to reach the same uncertainty of the WEP test.

Due to the different recoil velocities, the two atom interferometers will cover slightly different trajectories. The related recoil phase terms can be suppressed by inverting the direction of momentum transfer for subsequent cycles and calculating the half difference [27]. This requires a sufficient homogeneity over the baseline of the atom interferometer. To reach $\Delta \eta = 10^{-13}$, the homogeneity requirements of $3 \times 10^{-11} \mathrm{s}^{-2}$ in GG and $5 \times 10^{-12}\ \mathrm{m}^{-1}\mathrm{s}^{-2}$ are compatible with Earth's contributions. The mass distribution of the experimental apparatus itself has to be designed appropriately to avoid contributions exceeding these thresholds.

Figure 1 illustrates this scaling by indicating the required GG level of characterization as a function of the starting differential velocity for various target accuracies of the WEP test parametrized by $\Delta \eta$. In principle, the GG could be characterized with the atom interferometer in a gradiometer mode [31]. It becomes clear that an inherently small differential velocity would relax the requirements for a GG knowledge or even make it obsolete. Consequently, the systematics assessment would be considerably relieved, especially in scenarios, where the GG might drift unpredictably. The figure suggests that with a characterization of the GG within its magnitude on ground (horizontal line), reaching state-of-the-art WEP test performances of $\Delta \eta = 10^{-13}$ with quantum objects requires a bias in differential velocities of a fraction of $\mu\mathrm{m\ s}^{-1}$. This proposal is motivated by the absence, to our knowledge, of appropriate methods to achieve this accuracy in a dual atomic launch.

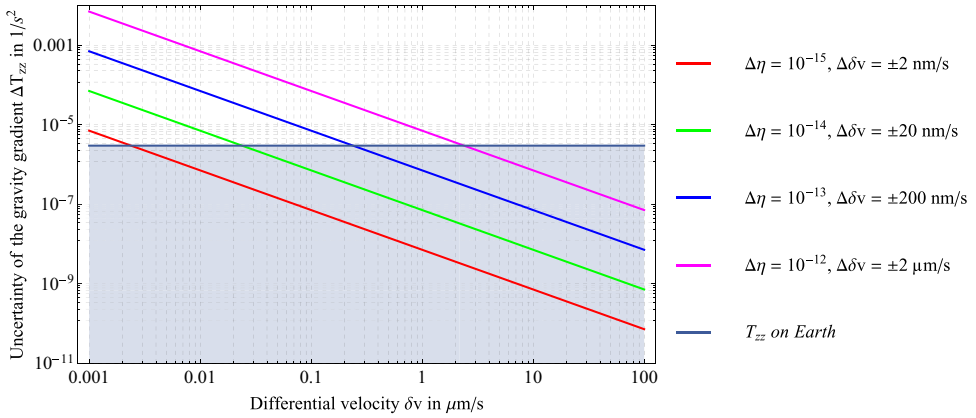

Figure 1. Required knowledge of the gravity gradient (GG) as a function of the inter-species differential velocity for several levels of performance $\Delta\eta$ of a WEP test. The case of a 10 m fountain is considered and implies an interferometry time of $2T = 2.74$ s. The interferometer is assumed to operate with two-photon transitions at about 780 nm each. Earth's GG affects the measurement and consequently needs to be determined in the shaded area. The corresponding differential acceleration is $\delta a = -T_{zz}(\pm\Delta T_{zz})\delta v_z(\pm\Delta \delta v_z)T$, where $\Delta\delta v_z$ denotes the uncertainty in differential velocity δv_z, and ΔT_{zz} denotes the uncertainty in GG T_{zz}. This leads to the plotted contribution to $\Delta\eta \propto \Delta T_{zz}\delta v_z$. For each curve, a maximum $\Delta\delta v_z$ is assumed (see legend) to keep, on ground, the other contributions (equation (5)) below the represented $\Delta\eta$.

To understand the origin of the differential velocity between two launched masses, we briefly recall the principle of a fountain launch. A lattice accelerated from $v = 0$ to $v = v_f$ induces a quantized momentum transfer via Bloch oscillations to an atom initially at rest. To avoid the population of multiple orders, the final lattice velocity v_f should match a targeted atomic velocity $N\hbar k/m$ where $N \in \mathbb{Z}$ with the modified Planck constant $\hbar$, the lattice light wave vector k and the atomic mass m. When the lattice transports two species of masses m_1 and m_2, the differential velocity at the end of the launch reads:

$$\delta v = \hbar k\left(\frac{N_1}{m_1} - \frac{N_2}{m_2}\right), \tag{6}$$

where N_1 and N_2 are the numbers of photon kicks transferred to species 1 and 2, respectively. From equation (6), it becomes clear that minimizing δv translates to finding a minimum of $(N_1/m_1 - N_2/m_2)$. With a single OL, choosing a final v_f matching a certain $\hbar k N_1/m_1$ completely fixes the choice of N_2. Thus, the bias δv cannot be minimized to better than a few tens of μ m s^{-1} in agreement with the predictions of [27] for the pair of isotopes ^{87}Rb and ^{85}Rb.

The idea of individually addressing each species with separate lattices is problematic since this would require vastly different ac-Stark shifts from each lattice. For sufficient lifetimes in the lattice however, high power and large detunings from the targeted electronic excitation are required. This generally means that other transitions, which are not much stronger detuned, e.g. of the other species, will have a considerable ac-Stark shift. Each lattice would have an effect on both species and the clean lattice dynamics are replaced by strongly time-varying potentials and undesired excitations. In this proposal, we solve this issue by choosing two lattices with *zero-magic* or *tune-out* wavelengths to selectively accelerate the two atomic clouds. At the start and the end of the acceleration phase, the wavepackets of different atomic masses m_1 and m_2 shall ideally have matching positions and velocities.

2. Scheme and method

For alkaline atoms, the contribution of the D_1 and D_2 lines to the dipole potential for one species of atoms reads [1]:

$$U_{\text{dip}}\left(\vec{r}\right) = \frac{\pi c^2}{2}\left[\left(\frac{\Gamma_{D_1}\left(1 - Pg_F m_F\right)}{\omega_{D_1}^3 \Delta_{D_1}}\right) + \left(\frac{\Gamma_{D_2}\left(2 + Pg_F m_F\right)}{\omega_{D_2}^3 \Delta_{D_2}}\right)\right] I\left(\vec{r}\right) \tag{7}$$

with $\Delta_{D_1} = \omega_{D_1} - \omega_L$ and $\Delta_{D2} = \omega_{D_2} - \omega_L$ are the detuning of the laser ω_L from the D_1 and D_2 atomic transition lines, respectively, and g_F is the hyperfine Landé factor. P is the polarization of the laser, m_F the Zeeman state of the atom and c the speed of light. When the atomic dynamic polarizability switchs sign between two resonances, a *magic-zero* or *tune-out* wavelength could be found [32–39]. Several magic-zero wavelengths have

Table 1. Magic-zero or tune-out wavelengths for alkaline atoms with neutralizing D_1 and D_2 contibutions according to equation (7). The variables P parametrizing the laser polarizations are assumed to be zero for simplicity. Theoretical calculations for alkaline-Earth-metal atoms are made in [35] and predict tune-out wavelengths for Be, Mg, Ca, Sr, Ba, and Yb to be 454.9813, 457.2372, 657.446, 689.200, 788.875, and 553.00 nm, respectively.

Isotopes	Γ_{D_1}(MHz)	Γ_{D_2}(MHz)	λ_{D_1}(nm)	λ_{D_2}(nm)	$\lambda_{\text{tune-out}}$(nm)	References
^{133}Cs	28.690	32.768	894.59295986	852.34727582	879.936574550	[43]
^{85}Rb	36.129	38.117	794.979014933	780.241368271	789.996623133	[44]
^{87}Rb	36.129	38.117	794.978851156	780.241209686	789.996461148	[45]
^{39}K	37.8684	37.8998	770.108385049	766.700921822	768.959724329	[46]
^{40}K	37.8998	37.8998	770.108136507	766.700674872	768.958845121	[46]
^{41}K	37.8998	37.8998	770.107919192	766.70045870	768.958628193	[46]
^{23}Na	61.353	61.542	589.7566617	589.1583264	589.557085633	[47]
^{6}Li	36.898	36.898	670.992421	670.977338	670.987393031	[48]

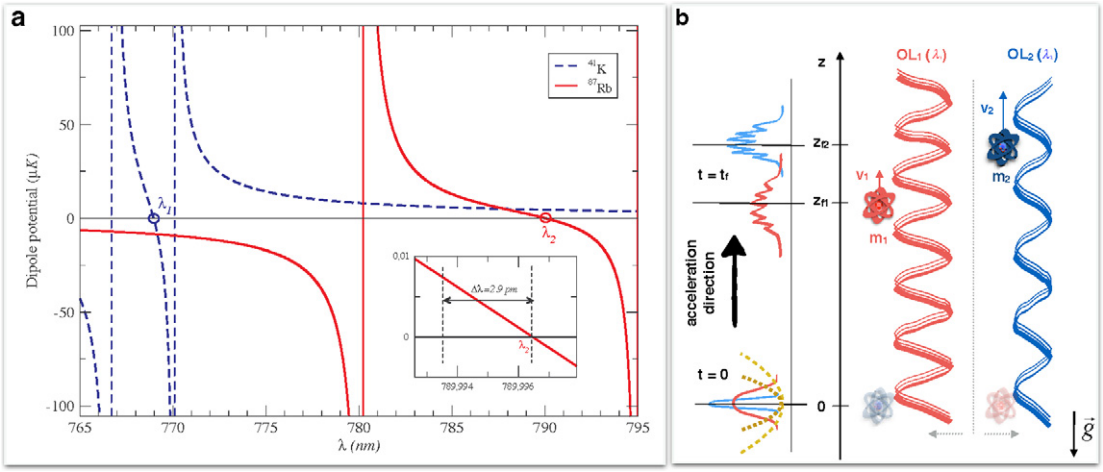

Figure 2. Selective lattice launch principle. (a) For each species the lattice wavelength is chosen as a tune-out wavelength of the other species. The two magic-zero values for rubidium and potassium are found at 789.9965 and 768.9586 nm, respectively. (b) The proposed arrangement makes it possible to selectively drive two kinds of atoms 1 and 2 by two optical lattices OL_1 and OL_2, respectively. This allows one lattice to bring one of the atomic clouds to any desired final position or velocity without altering those of the other species. In order to reach the precision target for this manuscript, a slight shift $\Delta\lambda$ from the rubidium magic wavelength is introduced (see inset) for the potassium lattice, leading to a small perturbation of rubidium dynamics.

been implemented in different experimental contexts [40–42]. In table 1, we provide some key values for commonly used alkalines and alkaline-Earth-metal atoms in the metrology context with identified tune-out wevelengths.

Recently very precise—uncertainty below 1 pm—measurements of these wavelengths were done for rubidium [49] and potassium [50]. We shall consider these two most used species in cold atoms laboratories as a study case to illustrate our method. Figure 1(a) shows that at the wavelength λ_1 (λ_2), the contributions of the two lines cancel out the dipole potential for ^{41}K (^{87}Rb). These special wavelengths were already implemented in mixture experiments to selectively manipulate ^{87}Rb and ^{41}K degenerate ensembles [51].

Based on these investigations, a magic-zero wavelength λ_1 could be used to create a lattice OL_1 accelerating the Rb cloud (species 1) without any effect on the ^{41}K atoms (species 2), and vice-versa with λ_2 (lattice OL_2), therefore realizing a dual-species fountain, which principle is illustrated in figure 2(b). The atomic ensembles are guided during the time t_f from the same initial position $z = 0$. OL_1 transports species 1 (in red) and OL_2 conveys species 2 (in blue) to $\{z_{f_1}, v_{f_1}\}$ and $\{z_{f_2}, v_{f_2}\}$, respectively. By choosing lattice acceleration ramps minimizing $z_{f_1} - z_{f_2}$ and $v_{f_1} - v_{f_2}$, we achieve a fountain launch that greatly relaxes the required knowledge of GG uncertainties as discussed in the previous section.

The simultaneous and independent use of lattices with two wavenumbers k_{L_1} and k_{L_2} allows for more flexibility towards cancelling $\delta\nu$, which reads now:

$$\delta\nu = \hbar \cdot \left(\frac{N_1 k_{L_1}}{m_1} - \frac{N_2 k_{L_2}}{m_2} \right). \tag{8}$$

After choosing a final velocity, thus the corresponding couple of integers N_1 and N_2, we could slightly tune one or both wavelengths to strictly reach a zero differential velocity. This is illustrated for the study isotopes case in

the inset of figure 2(a) by the shift $\Delta\lambda = 2.9$ pm corresponding to $\Delta k = 29.22\ \mathrm{m}^{-1}$ from the tune-out value k_{L_2}. This comes at the price of introducing a perturbation by OL_2 to the dynamics of the ^{87}Rb cloud which now is subject to the accelerating effect of this lattice ramped in time to transport ^{41}K. In the following sections, numerical simulations are implemented to check whether this parasitic contribution affects the fidelity and performance of the selective acceleration process.

Both chosen species ^{87}Rb and ^{41}K have positive scattering lengths: 99 a_0 and 60 a_0, respectively, where a_0 is the Bohr radius. They can be cooled down to degeneracy independently [52] or taking advantage of sympathetic cooling [53]. Another advantage of this pair in the context of precision measurements is the existence of a low-magnetic field (79 G) Feshbach resonance allowing to tune the inter-species interaction to zero [40] and maximize the overlap between the two BECs while in the Zeeman state $F = 1, m_F = 1$. This manipulation is very useful since inter-component interactions lead otherwise to a shell structure (in the case of the chosen isotopes) or could in immiscible phases form mixture ground states with broken spatial symmetry. Both of the last geometries lead to complex and coupled expansion dynamics of the BECs, thus to significant wave fronts-related systematic effects. These effects being leading systematics in most atom interferometry experiments, it is vital for precision differential atom interferometry to minimize or neutralize the inter-species interactions. This motivates our choice to consider in this study the intra-species interactions only. As a consequence, during the proposed acceleration ramps, the atoms are assumed to remain in magnetic sensitive sub-states. Couplings to the Feshbach field lead to magnetic field gradients and induce a differential velocity due to the different atomic properties. In principle, a characterization of the gradients could be performed by dedicated measurements with the atom interferometer [54] and the resulting differential velocity cancelled by accounting for it in the proposed lattice launch sequence. Assuming a time 10 ms before transfer to the magnetically insensitive states and switching-off the Feshbach field, the magnetic field gradient should be below 1 mG m^{-1} in average to reach $\Delta\eta = 10^{-13}$ or 10 μG m^{-1} to reach $\Delta\eta = 10^{-15}$.

3. Theoretical model

Justified by the cancelled inter-species interactions, the treatment is described for one species and could be applied to the other simply by accounting for its different temporal control sequence of external potentials. The momentum shift $\Delta k = 29.22\ \mathrm{m}^{-1}$ chosen to perfectly match the two final velocities leads to a parasitic contribution of OL_2 in the dynamics of species 1 (lattice depth of few nK). Moreover, the assumed finite uncertainty in the definition of the tune-out wavelengths (1 pm) leads to a small ac Stark effect even in the case of the atoms for which it should be magic-zero. None of these effects is neglected by solving the dynamics equations of both BECs in presence of the two lattice potentials weighted by their exact numerical magnitude.

3.1. Gross–Pitaevskii equations (GPEs)

In the mean-field regime, a BEC is well described by the GPE. This often-called nonlinear Schrödinger equation features an additional term describing the interactions between atoms. At low temperature, the system of N bosons is described by a single wavefunction $\Psi(\mathbf{r})$ [55] solution of the stationary GPE:

$$\left[-\frac{\hbar^2}{2m}\nabla^2 + V(\mathbf{r}) + Ng_{3\mathrm{D}}\,|\Psi(\mathbf{r})|^2\right]\Psi(\mathbf{r}) = \mu\Psi(\mathbf{r}), \tag{9}$$

where m is the mass of the bosonic species considered, $V(\mathbf{r})$ the external potential seen by the atoms and μ is the chemical potential. The magnitude of the nonlinear term is proportional to the total number of condensed bosons N and the atom–atom interaction magnitude. When assuming s-wave scattering only, the interaction term reads

$$g_{3\mathrm{D}} = \frac{4\pi\hbar^2 a_s}{m}, \tag{10}$$

where a_s is the s-wave scattering length of the atomic species. In this proposal, we consider atomic species with repulsive interatomic interactions. In a fountain configuration, the relevant physical effects (acceleration, center-of-mass motion, etc) triggered by the lattice accelerating potentials V_{OL_1} and V_{OL_2} occur mainly in the gravity direction z justifying a one-dimentional treatment. The ground state of the problem is found by solving the effective one-dimensional GPE

$$\left[-\frac{\hbar^2}{2m}\frac{\partial^2}{\partial z^2} + \frac{1}{2}m\omega_z^2 z^2 + Ng_{1\mathrm{D}}\,|\Psi(z)|^2\right]\Psi(z) = \mu_{_{1\mathrm{D}}}\Psi(z), \tag{11}$$

where $g_{1\mathrm{D}}$ and $\mu_{1\mathrm{D}}$ are the effective 1D interaction strength and chemical potential, respectively.

The time-dependent behavior of the BEC before and during vertical acceleration, is followed while solving the time-dependent GPE

$$i\hbar\frac{\partial}{\partial t}\Psi(z,\,t)=\Bigg[-\frac{\hbar^2}{2m}\frac{\partial^2}{\partial z^2}+\frac{1}{2}m\omega_z^2(t)z^2+V_{\mathrm{OL}_1}(z,\,t)+V_{\mathrm{OL}_2}(z,\,t)+Ng_{1\mathrm{D}}\,|\Psi(z,\,t)|^2\Bigg]\Psi(z,\,t), \tag{12}$$

where $\omega_z(t)$, $V_{\mathrm{OL}_1}(z,\,t)$ and $V_{\mathrm{OL}_2}(z,\,t)$ are time-dependent potentials accounting for a complete sequence of loading a BEC from a harmonic trap into two OLs that accelerate it.

3.2. Loading, release and acceleration ramps

During any fountain launch proposed in this manuscript, The total potential reads:

$$V(z,\,t)=\begin{cases}V_{\mathrm{loading}}(z,\,t), & \left[t_0,\,t_1\right]\\ V_{\mathrm{acc}}(z,\,t), & \left[t_1,\,t_4\right]\\ V_{\mathrm{switch-off}}(z,\,t), & \left[t_4,\,t_5\right].\end{cases} \tag{13}$$

The expressions taken by the potential at each time step are presented in the following.

Loading and release In order to adiabatically load a BEC in the OLs considered, the magnitude of their potentials is increased smoothly. We model this step by multiplying the potential with the function $f_{\mathrm{ON}}(t)$ defined as follows:

$$f_{\mathrm{ON}}\left(t;\,t_{\mathrm{ON}},\,\tau\right)=\begin{cases}\sin^2\left(\frac{1}{2}\frac{\pi}{\tau}\left(t-t_{\mathrm{ON}}\right)\right) & ,\left[t_{\mathrm{ON}},\,t_{\mathrm{ON}}+\tau\right]\\ 1 & ,\,t>t_{\mathrm{ON}}+\tau,\end{cases} \tag{14}$$

where t_{ON} denotes the starting time of ramping up the lattice and the characteristic loading duration is set by τ. A complementary behavior regulates an adiabatic switch-off through the function:

$$f_{\mathrm{OFF}}\left(t;\,t_{\mathrm{OFF}},\,\tau\right)=\begin{cases}\cos^2\left(\frac{1}{2}\frac{\pi}{\tau}\left(t-t_{\mathrm{OFF}}\right)\right), & \left[t_{\mathrm{OFF}},\,t_{\mathrm{OFF}}+\tau\right]\\ 0, & t>t_{\mathrm{OFF}}+\tau.\end{cases} \tag{15}$$

During the loading phase, the initial harmonic trap is switched off while the lattices are ramped up. We label this time interval $[t_0, t_1]$. After acceleration, the BEC is released adiabatically in order to recover its single-peaked distribution in momentum space. This step is performed over the time interval $[t_4, t_5]$. The total external potential for a species of atoms within these initial and final steps reads:

$$V_{\mathrm{loading}}\left(z,\,t_0<t<t_1\right)=f_{\mathrm{OFF}}\left(t;\,t_{\mathrm{OFF}}=t_0,\,\tau\right)\left[\frac{1}{2}m\omega_z^2z^2\right]+f_{\mathrm{ON}}\left(t;\,t_{\mathrm{ON}}=t_0,\,\tau\right)\left[\frac{V_1}{2}\left(1+\cos\left(2k_1z\right)\right)+\frac{V_2}{2}\left(1+\cos\left(2k_2z\right)\right)\right], \tag{16}$$

and

$$V_{\mathrm{switch-off}}\left(z,\,t_4<t<t_5\right)=f_{\mathrm{OFF}}\left(t;\,t_{\mathrm{OFF}}=t_4,\,\tau\right)\left[\frac{V_1}{2}\left(1+\cos\left(2k_1\left(z+v_{\mathrm{OL}_1}^f t+c_{\mathrm{OL}_1}^f\right)\right)\right)+\frac{V_2}{2}\left(1+\cos\left(2k_2\left(z+v_{\mathrm{OL}_2}^f t+c_{\mathrm{OL}_2}^f\right)\right)\right)\right], \tag{17}$$

with $v_{\mathrm{OL}_{1(2)}}^f$ and $c_{\mathrm{OL}_{1(2)}}^f$ being velocities and offset positions of the lattice 1(2) at the end of the ramp, respectively. They are determined by the choice of the target final velocities of the atoms as explained in the next paragraph. Depending on the study case, we could choose the same or different values of τ in the different temporal functions f_{ON} and f_{OFF}.

Acceleration ramps. In order to accelerate the condensates without leaving the first band, the OLs must be tuned on and off adiabatically. A common method of doing this is to use the following lattice acceleration profile $a(t)$ during a time sequence $[t_0, t_5]$:

$$a(t) = \begin{cases} 0 & , \left[t_0,\, t_1\right] \\ a_{\max}\frac{\left(t-t_1\right)}{\triangle t} & , \left[t_1,\, t_2\right] \\ a_{\max} & , \left[t_2,\, t_3\right] \\ -a_{\max}\frac{\left(t-t_4\right)}{\triangle t} & , \left[t_3,\, t_4\right] \\ 0 & , \left[t_4,\, t_5\right]. \end{cases} \tag{18}$$

This sequences determines the lattice phases. Once the common target final velocity and the acceleration sequence duration are chosen, one needs to determine the constant acceleration $a_{\max}$ and the different time intervals of the acceleration sequence. To find out these characteristic times, we choose a couple of total numbers of recoils cancelling δv in equation (8) and a value of $a_{\max}$ for each species that is not too large for an optimal acceleration [56]. Typical experimental realizations involve about 2000 m s^{-2}. Based on the trapezoidal geometry of the ramp, the total number of recoils gained by one species $N_{\text{kicks}} = \frac{1}{v_r}\int_{t_1}^{t_4} a(t)\,\mathrm{d}t$ is the sum of three intervals contributions:

$$N_{\text{kicks}} = \begin{cases} \frac{1}{v_r}\frac{a_{\max}}{2}\triangle t & , \left[t_1,\, t_2\right] \\ \frac{1}{v_r}a_{\max}\triangle T & , \left[t_2,\, t_3\right] \\ \frac{1}{v_r}\frac{a_{\max}}{2}\triangle t & , \left[t_3,\, t_4\right], \end{cases} \tag{19}$$

where $v_r = \hbar k/m$ is the recoil velocity of one of the species of mass m driven by the OL of wave vector k. In general, a different choice of $\triangle t$ (or t_2 and t_3) and $a_{\max}$ for each species could be done leading to a different phase in the time-dependent potentials parametrized with the position offset between the two OL previously introduced in equation (17) by $c^f_{\text{OL}_{1(2)}}$. We choose $\triangle t$ and $a_{\max}$ for both sequences such that the two initially co-located minima of the two different OL do not shift at the end of the sequence by more than the maximum displacement of the BECs centers allowed by the WEP test performance targeted. In the case of a measurement of η to the 10^{-15} level, this offset would be about 1 nm. We check that this threshold is not crossed when engineering the ramp sequences and choosing the couples $\triangle t$ and $a_{\max}$ corresponding to $v^f_{\text{OL}_1} = v^f_{\text{OL}_2} = N_1\hbar k_1/m_1 = N_2\hbar k_2/m_2$. Finally, the total potential exerted on one species during the acceleration phases reads

$$V_{\text{acc}}\left(z,\, t_1 < t < t_4\right) = \frac{V_1}{2}\left[1 + \cos\left(2k_1\left(z + z_{\text{OL}_1}(t)\right)\right)\right] + \frac{V_2}{2}\left[1 + \cos\left(2k_2\left(z + z_{\text{OL}_2}(t)\right)\right)\right], \tag{20}$$

where $z_{\text{OL}_{1/2}}(t)$ are completely set after the choice of t_1, t_2, t_3, t_4 and $a_{\max}$ for each of the lattices $\text{OL}_{1/2}$.

We would like to stress out that due to the deliberately introduced shift Δk, it is not guaranteed that the effect of the magic-zero lattice OL_2 on species 1, which magnitude scales with V_2, is negligible. Any effect on the center of mass and momentum distribution of BEC 1 would set a limit on our proposed method. This is essentially the motivation for the in-depth numerical simulations made, the results being detailed in the Results section.

3.3. Frame transformation

The typical realizations we would like to model involve tall fountains of 10 m or more. Corresponding acceleration ramps would accelerate the BECs over distances of few cm. To efficiently treat this problem numerically, we employ a moving frame description, reducing the required grid extension. All of the dynamics takes place around the translated center of the BECs, which in the ideal case follows closely the trajectory z_{OL} of the accelerated OL. We take advantage of this situation to perform a transformation to an accelerated co-moving frame with the OL. This classical so-called extended Galilean transformation [57–59] takes the system from (z, t) to transformed coordinates (Z, T), where

$$\begin{cases} Z = z - z_{\text{OL}}(t) \\ T = t. \end{cases} \tag{21}$$

Applying this transformation, a term proportional to $\dot{z}_{\text{OL}}$ and the first derivative of the wave function appears in the GPE. The phase transformation

$$\Psi(Z,\, T) = \mathrm{e}^{-\left(\frac{\mathrm{i}}{\hbar}Zm\dot{z}_{\text{OL}}\right)}\Phi(Z,\, T) \tag{22}$$

makes it vanish. After a transformation of all operators in the accelerated frame, the time-dependent GPE reads

$$\mathrm{i}\hbar\frac{\partial}{\partial T}\Psi(Z,\,T)=\left[-\frac{\hbar^2}{2m}\frac{\partial^2}{\partial Z^2}+V_{\mathrm{OL}_1}(Z,\,T)+V_{\mathrm{OL}_2}(Z,\,T)+Ng_{1\mathrm{D}}\,|\Phi(Z,\,T)|^2+Zm\ddot{z}_{\mathrm{OL}}\right]\Psi(Z,\,T). \quad (23)$$

The advantage of this system of coordinates becomes clear when writing the transformed accelerating potential terms (20) to

$$V_{\mathrm{acc}}\left(Z,\,t_2<t<t_4\right)=\frac{V_1}{2}\left[1+\cos\left(2k_1(Z)\right)\right]+\frac{V_2}{2}\left[1+\cos\left(2k_2\left(Z+z_{\mathrm{OL}_2}(t)-z_{\mathrm{OL}_1}(t)\right)\right)\right], \quad (24)$$

where the choice is made here to center the grid on z_{OL_1}. Since the two accelerated lattices of the problem are not allowed to acquire a large position offset all along the acceleration sequence, the term $z_{\mathrm{OL}_2}(t)-z_{\mathrm{OL}_1}(t)$ appearing in (24) does not lead to a need for a larger grid than the one centered on z_{OL_1}.

3.4. Numerical techniques

The method used to find the ground state and dynamics of the condensates is based on a split-operator treatment initially reported in [60] and previously applied in a similar context in [61, 62]. It consists in breaking the evolution operator within a time step δt in a product of two kinetic propagators separated by a potential one. The Hamiltonian is assumed to be time-independent during this time step and the error made during it scales with $(\delta t)^3$. The potential propagator is applied in a straightforward way to the wave function whereas the kinetic one is only diagonal in the momentum space. For each application of the latter, the BEC wave function is transformed to the momentum space beforehand. Transforming back and forth from these spaces is done using an optimized fast Fourier transform (FFT) developed by Intel for FORTRAN compilers [63]. Finding out the ground states is done following the same recipe but in complex time [64]. Typical grids used feature 2^{17} points and extend over 700 μm. A full loading and acceleration sequence of about 10 ms requires a numerical propagation of few hours on a standard desktop computer (Intel i5 processor with 8 GB RAM).

4. Results

4.1. Loading to and release from the OL

As previously stated, the choice of a long enough time τ is crucial to allow an adiabatic transfer of the BECs from their initial harmonic traps to the OLs and at the release step. In order to stress out the dramatic effect of this choice, we contrast in figure 3 the extreme case of a sudden switch-on and -off of the lattice potential ($\tau=0$) with an adiabatic ramping.

The gallery shows the BEC momentum distribution at three different times (i) in the harmonic trap just before loading in the OL, (ii) after loading and (iii) after release from the OL. A too short or zero value of τ leads to a released BEC with several momentum classes populated (blue dashed peaks at $\pm 2\hbar k$ in figure 3(c)). This effect is limiting the population of the chosen momentum at the end of the ramp thereby reducing the number of atoms involved in the AI. An adiabatic loading and release at $\tau=80$ μs (red plain curve) guarantees a single-peaked density in momentum space $|\Psi(k)|^2$ after release from the lattice. This is observed in both cases of a static or accelerated lattice. The sequences considered in this manuscript are all characterized by a choice of τ guarantying a final single momentum peak, thus a maximum efficiency of the coherent transport.

4.2. Dual-species launch

In this section, we illustrate the implementation of the dual-fountain launch by propagating the two BECs using the ramps shown in figure 4(a). We choose to imprint 2280 and 1104 kicks for ^{87}Rb and ^{41}K. This choice would drive the atoms to acquire a final velocity of 13.6 m s^{-1} realizing a fountain of about 10 m as planned in three facilities so far [24–26]. After the acceleration phase, the two BECs are transferred to the exact target momentum class as shown in figures 4(c) and (e) (red and blue dashed lines) and spatially lifted off to the same height of 5.5 cm (figures 4 (b) and (d)). The fidelity of this process is subject to a final adiabatic release from the OLs. A sudden or imperfect release leads to the a loss of atoms in other momentum classes ($\pm 2\ \hbar k$, $\pm 4\ \hbar k$ and $\pm 6\ \hbar k$ (black plain lines in (b) and (d)).

To check, in the adiabatic loading and release case, if the acceleration process is free from parasitic effects caused by the simultaneous application of two OLs, we zoom-in in figure 5 around the central and unique momentum peaks obtained. Whereas the effect of the presence of two lattices is negligible for ^{41}K as expected (lower graph), it is clearly visible that it amplifies the fluctuations around the maximum of the ^{87}Rb momentum distribution. This stems from the use of two OL in the latter case where both are not at the *magic-zero* wavelengths. The parasitic effect of OL_2 seems, however, to be simply modulating the momentum distribution around the targeted central value in a symmetric fashion. The numerical analysis conducted in the next sections will confirm this statement. Such a perturbed but symmetric momentum distribution (around the target value)

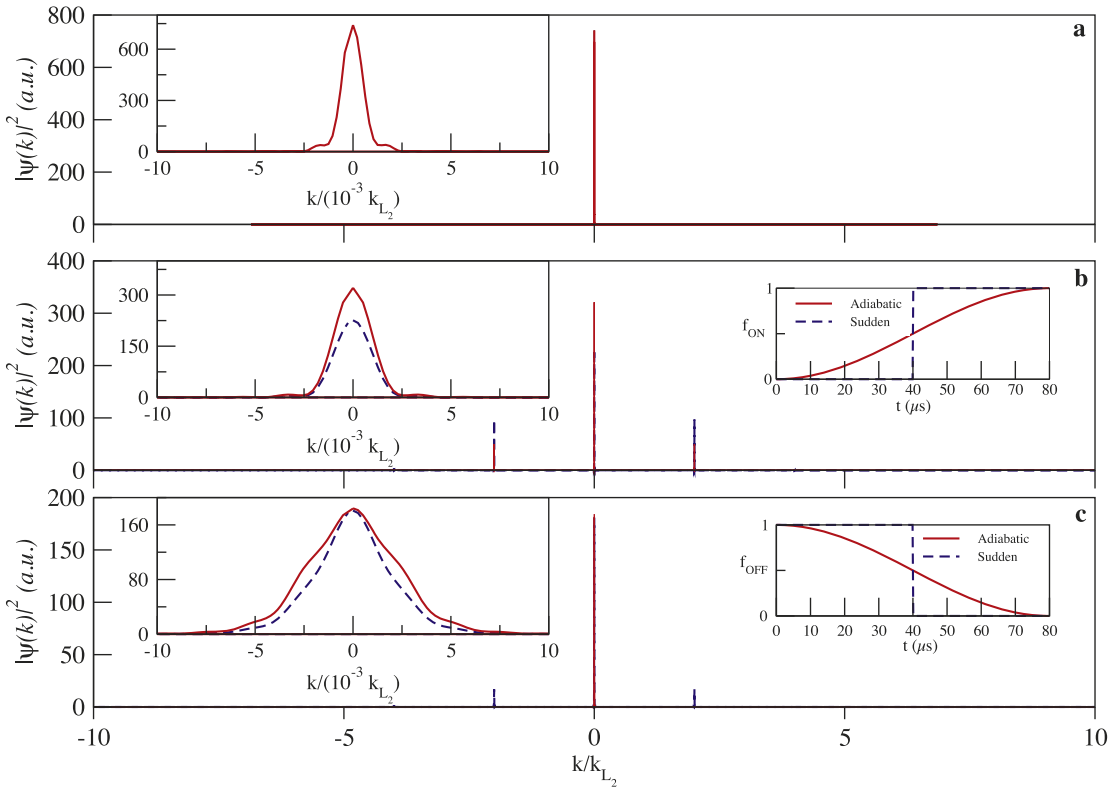

Figure 3. Momentum distribution $|\Psi(k)|^2$ of a ^{41}K Bose–Einstein condensate of 10^5 atoms in units of $\hbar k_{L_2}$. (a) Initially trapped BEC in a harmonic potential with orbital frequency $\omega_z = 2\pi$ 5 Hz. The interactions magnitude are chosen equal to the case where a transverse orbital frequency of 2π 500 Hz would be applied. (b) Momentum distribution after loading in a lattice of wavelength λ_2 and depth $s = 4.7$ (c) released wave functions after a free expansion in the optical lattice of 0.24 ms. The right-hand insets show the switching-on and -off functions f_{ON} and f_{OFF} used in both the sudden (dashed lines) and adiabatic (plain lines) cases. The left-hand insets are a zoom at a different scale on the central peak of every graph. The outcome of an adiabatic loading and release at $\tau = 80$ μs is characterized by a single peak (red plain curves) suggesting that all atoms remained in one momentum class.

would not lead to an additional dephasing in a WEP test since the differential velocity between the two BECs relies solely on the centers of the momentum wave packets at the input of the dual interferometer.

4.3. Dual-lattice dynamics and role of the interactions

To interprete the momentum density distribution of ^{87}Rb, we contrast in figure 6 the cases of an acceleration following the ramps previously applied (right column) and a simple expansion lasting for the same duration (left column) for different regimes of interactions. In all numerical experiments, the ^{87}Rb BEC wave packets are released adiabatically from the OLs. The first row (a) and (b) shows that the BEC loaded in OL$_1$ has the same momentum density whether accelerated by this lattice or simply expanded in it for the same time. The momentum width in both cases is, however, larger than the initial one (by a factor of 10 to 20) driven by interaction dephasing over the lattice sites. Indeed, depending on the number of atoms per site, the chemical potential leads to different phase winding in every lattice well. This causes momentum broadening even in the case where atoms are loaded and released adiabatically [65, 66]. When Bloch oscillations are involved, atomic interactions lead to a dephasing and a broadening of the quasi-momentum width as observed in [67] and analyzed in [68]. Recently, the same effect was observed in the context of a metrology-oriented lattice-accelerated BEC experiment [69]. In [68], the increase in momentum width is proportional to $\sqrt{g_{1D}} \cdot t$), where t is the evolution time. By varying the number of atoms in the BEC or the time spent in the lattice, we could check that our results are consistent with this scaling in the case of a simple expansion in the lattice. Since the momentum width of a wave packet is a critical quantity for the contrast of an atom interferometer [70], it is of interest to keep it as low as possible. This can be realized by utilizing delta-kick cooling techniques [69, 71–73] or by taking advantage of the existence of Feshbach resonances to tune down the interactions magnitude. The next row (c) and (d) illustrates the case when two OLs are in presence and shows that the main perturbation and broadening of the momentum peak stems from the evolution in the bichromatic lattice configuration imposed to ^{87}Rb. Although, the second lattice OL$_2$ is several orders of magnitude weaker than the main accelerating one, it introduces a dephasing of the atomic cloud spatially extending over bichromatic lattice sites starting co-located at the origin but with potential minima that spatially separate the further the atoms are off-centered from $z = 0$.

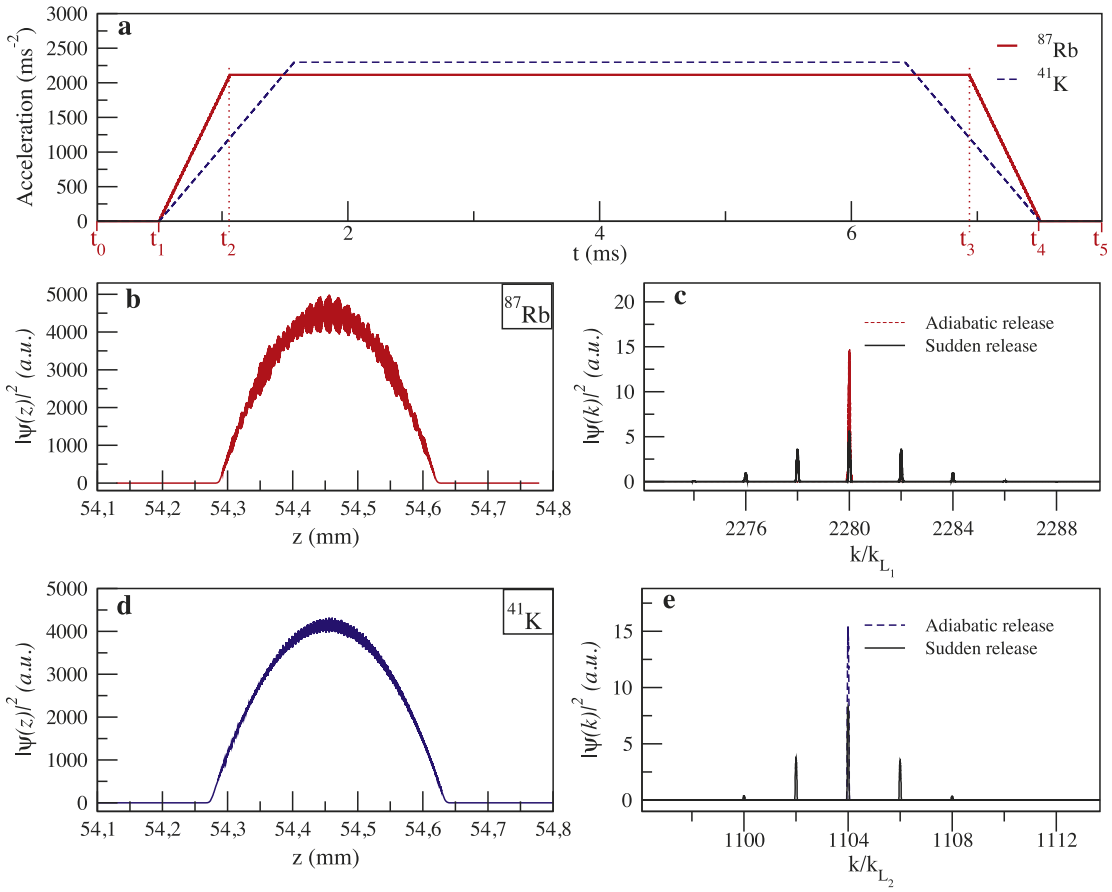

Figure 4. Species-selective 10 m fountain for ^{87}Rb and ^{41}K BECs. (a) Acceleration ramps for the two species with the key time points indicated for the rubidium case (solid red line) as labeled in the theoretical model section. (b) and (d) Position space probability densities of the two condensates accelerated in less than 8 ms to a common height of about 5.5 cm. (c) and (e) The acceleration ramps bring the BECs to the target momentum class (red and blue dashed central peaks) corresponding to a velocity of 13.6 m s^{-1}. The importance of an adiabatic release is highlighted by contrasting it to the case of a sudden switch-off of the two OLs. In the latter case, parasitic velocity states (side peaks) are populated leading to a loss in the usefully accelerated atoms. For this simulation, we considered 10^4 atoms in each BEC with timing ramps corresponding to 1104 for (^{41}K) and 2280 for (^{87}Rb) momentum kicks transferred in units of the respective k_L. The depths of the acceleration lattices used are $s_1 = V_1/E_{R_1} = 104$ for rubidium and $s_2 = V_2/E_{R_2} = 31$ for potassium, $E_{R_i} = \hbar^2 k_i^2/(2m_i)$ being the respective recoil energies for species $i\,(i = 1, 2)$.

By contrasting (c) and (d), it becomes clear that the accelerated case with different ramps applied to the two OLs leads to an averaging of this dephasing effect reducing perturbations and broadening of the momentum density distribution. Since the case of graph (d) is the one of interest in this article, the suitability of our proposal is confirmed. It is obvious that the size of the wave function during the expansion or acceleration process is a key quantity to account for since it determines the lattice sites occupancy. The size being shaped, in the BEC case, by the atomic interactions, it is necessary to clarify and distinguish the roles of size and interactions. To this end, we plot in the lower row (e) and (f), the momentum densities of the ^{87}Rb BEC with tuned-off interactions. In plot (e) and for the case of two lattices, we start with the same BEC wave function (same initial extension than the one in plot (c) before switching off the interactions for the complete evolution time. This suggests that, initially, the same number of bichromatic lattice sites are occupied. The similarity in the behavior of the two momentum structures (same peaks each $2 \cdot (k_{L_1} - k_{L_2})$ and relative magnitude than (c) confirms our interpretation of the dephasing due to more spatial separation between the sites of OL_1 and OL_2. The interactions in the case (c) simply broaden every momentum peak already visible in (e). When a single lattice is present (black plain curves of graphs (e) and (f), the broadening of the initial ground state observed in (a) and (b) disappears with the vanishing interactions. In this case, the local lattice sites density does not play any role in altering the overall BEC phase. As for (a) and (b), there is no difference whether the BEC is accelerated or kept expanding in the lattice. The broadening observed in the expanding case of the bichromatic static lattice (red dashed curve in (e) is averaged out (red dashed in (f)) thanks to the different accelerating ramps and matches the single lattice case (solid black curve in (f)). As a conclusion, two effects are altering the momentum distributions of the BECs: (i) momentum broadening driven by interactions dephasing with complex shapes of the envelopes and (ii)

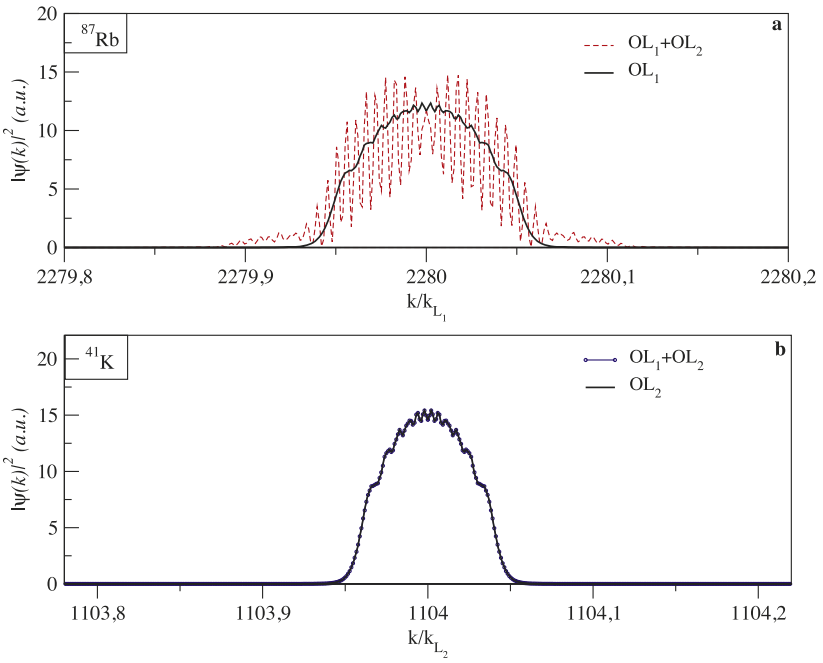

Figure 5. Zoom on the single momentum peaks of the accelerated Bose–Einstein condensates. This figure is a zoom on the momentum distribution in the adiabatic release limit of figures 4(c) and (e). (a) The effect of the concurrent application of OL_1 and OL_2 on ^{87}Rb condensate is modulating the momentum density around the central target value in a symmetric way. (b) The ^{41}K condensate density in momentum space remains unaffected (compared to a single lattice case) since OL_1 is exactly the magic-zero wavelength for this atom.

bichromatic lattice dephasing, however, averaged out by the different acceleration ramps proposed in our scheme.

4.4. Effect of the number of kicks

In the case of the proposed scheme, the parasitic effects discussed above do not seem to be related to the number of momentum kicks transferred. It is, however, important to check if the fidelity of the process is harmed for higher velocity ramps. Indeed, if it is the case, the dual-lattice dephasing will add up for longer sequences or taller fountains setting a limit on the practically realizable interferometry times. Figure 7 does not support the occurrence of such effects. Comparing the momentum probability density of the two species (upper and lower rows) for largely different accelerations (left versus right column), we observe no difference in the shape or density magnitude of the wave functions. Numerical estimations of the differential velocity between the two species confirm this statement. This demonstrates the scalability of the method since no detrimental effects are observed for longer baselines. Only realistic experimental constraints are expected to set a limit to the proposed dual-species launch as homogeneity of the optical or magnetic traps involved.

4.5. Quantitative evaluation of the differential velocity

The minimum differential velocity between the two species is solely limited by the effect of the potassium lattice perturbing the rubidium atoms distribution, being non-magic-zero. In order to evaluate this effect, we estimate the velocity difference of rubidium when the second lattice is present compared to the ideal case of OL_1 alone. The analogous effect of OL_1 on potassium is strictly absent since its wavelength is exactly the magic-zero one. By changing the power of OL_2, we estimate in figure 8 the bias velocity offset of the ^{87}Rb BEC from the reference ideal one of 2280 $\hbar k_{L_1}/m_1$. For an OL_2 beam waist of 1 mm, The perturbation starts to be important for several Watts. Keeping the lattice power between typical experimental values of 0.5 and 1 W, we bound the velocity perturbation below the low limit (few tens of nm s^{-1}) identified for the high-precision measurements motivating the actual proposal. Within this range of parameters, the inter-species differential velocity lies similarly around few tens of nm s^{-1}. To match the launching velocities on a level of μm s^{-1} (nm s^{-1}) for $\Delta\eta = 10^{-13}$ [10^{-15}], the lattice frequencies have to be controlled to 0.1 GHz [0.1 MHz], which can be done e.g. by a frequency comb. Assuming retro reflected lattices, the relative angle between the lattices has to be below 40 μrad to allow for maximum differential velocities of nm s^{-1}. A mitigation strategy is using common optics for both lattices. The method adopted to evaluate these velocities was to find the expectation values of the momentum operator for each of the BECs and compare them. The finite velocity width implies a statistical

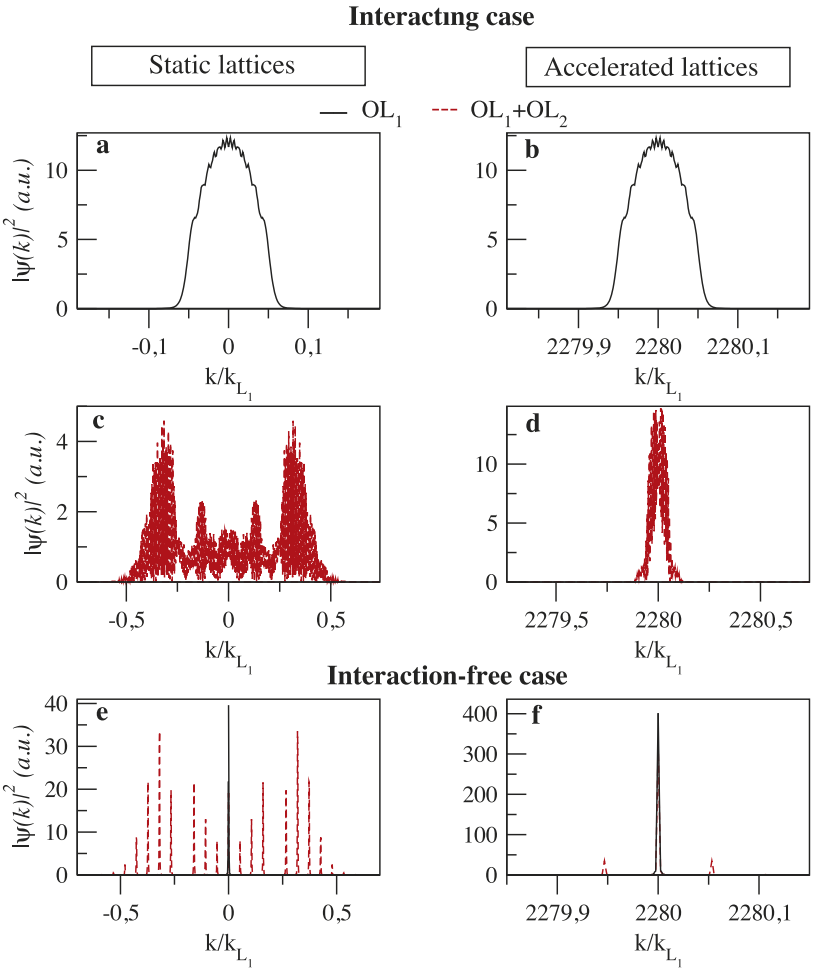

Figure 6. Expansion of the ^{87}Rb BEC for various situations after an adiabatic release from the involved lattice(s). The final wave-function is shown for a single lattice OL_1 (solid black) and with a second one (OL_1+OL_2) (dashed red). The effects of lattice(s) acceleration (right column) are contrasted with static lattice(s) (left column). (a) and (b) The proposed acceleration ramp in a single lattice does not lead to a broadening of the momentum distribution. (c) and (d) The evolution of the BEC in the bichromatic lattice potential (OL_1+OL_2) leads to a broadening of the momentum distribution due to dephasing occurring between multiple bichromatic lattice sites. This effect is dramatically reduced in the accelerated case (d) as we chose slightly different acceleration ramps for the two lattices, causing the perturbation in each site to oscillate and average down. (e) Even with vanishing interactions, the same BEC structure than case (c) is observed for the bichromatic lattice case. The dephasing effect leads to the same momentum peaks (with less broadening) and relative magnitudes. (f) The different acceleration ramps make the bichromatic dephasing average down and we observe the same momentum distribution for one or two lattices. Note that the BECs of (b) and (d) are the same plotted in figure 5(a).

uncertainty in the center of mass velocity. Coupled to GGs this leads to a noise contribution in the interferometer which has to be kept below the shot noise limit. For 10^6 atoms of each species, two photon beam splitters, contrasts near unity, a free evolution time of $T = 1.37$ s, Earth's GG, and velocity widths as depicted in figure 5 the related noise would be smaller than the shot noise by one order of magnitude. The differential center of mass motion can be assessed by spatially resolved imaging directly after launch and subsequently after $2T$. Repeating these measurements for about 20 times is sufficient to reach the precision required for a target of $\Delta\eta = 10^{-13}$. Higher precisions require either a higher number of measurements or a reduction in velocity width. Even in a space-borne experiment and assuming the parameters from [74], the noise associated with the statistical uncertainty in the center of mass velocity would be below the anticipated shot noise limit.

5. Conclusion and discussion

In this article, the idea of using two OLs at the zero-magic wavelengths of ^{87}Rb and ^{41}K allowed to manipulate each of them selectively. The motivation behind this scheme is to achieve a perfectly zero inter-species differential velocity required in precision tests of the WEP in fountain geometries. To the best of our knowledge, no acceleration method of two different atoms or isotopes to a common precise velocity was reported so far. In order to strictly cancel the differential velocity between the species, one of the lattices had to be slightly shifted leading to a perturbing effect on one of the atoms (^{87}Rb). Numerical simulations of the dynamics of two BECs of

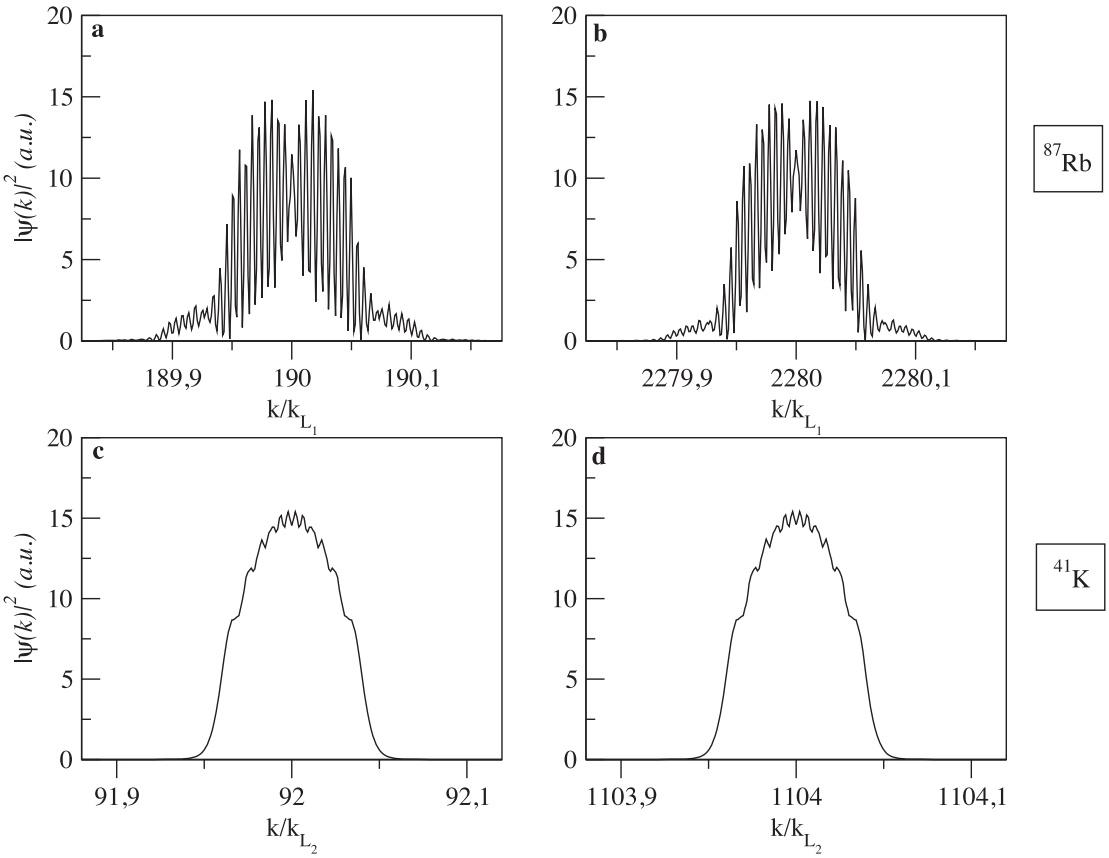

Figure 7. Effect of the number of momentum kicks. The right column differ from the left one by more than one order of magnitude in the total number of momentum kicks transferred. The upper panel illustrates the ^{87}Rb case whereas the lower ones corresponds to the acceleration of the potassium 41 isotope. This figure demonstrates the scalability of the method since different fountains of variable sizes could be operated using the same principle. No alteration of the momentum of the launched species is observed whether the fountain realized is few tens of cm or has a height of 10 m. Note that the duration of the two ramps (less than 8 ms) is chosen to be the same in the two cases (left versus right) in order to decouple the effect of momentum transfer from interaction dephasing effects, which scale linearly with time [68].

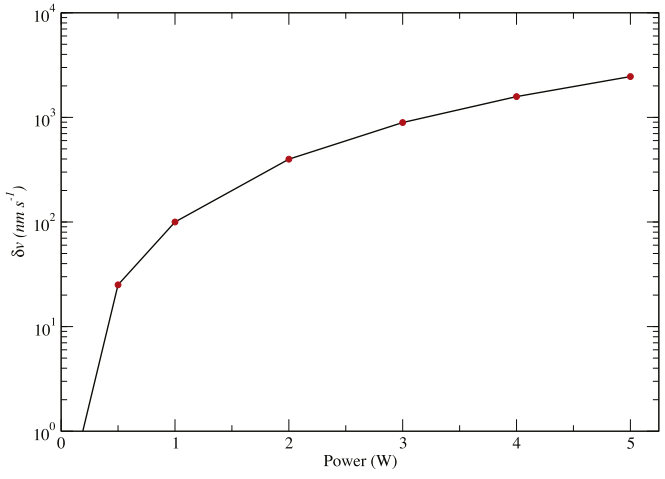

Figure 8. Velocity offset (from the ideal value) in the case of the ^{87}Rb BEC as a function of the power of the non-magic-zero lattice. The offset is compared to the reference value of 2280 $\hbar k_{L_1}/m_1$ and plotted against the power of the perturbing lattice OL_2. Since the lowest differential inter-species velocity is limited by the effect of OL_2 on ^{87}Rb, the velocity offset introduced for this species is the relevant quantity to compare with the target differential velocity between the species. The waist of the dipole lasers forming the lattice is chosen to be 1 mm for all the simulated cases of this figure. It is clear that for typical experimental values of the power of OL_2 (about 0.5 W), the systematic velocity offset introduced is about 10 nm s^{-1} required in high-precision tests.

the above-mentioned atoms with realistic parameters lead to the conclusion that this perturbation does not alter the efficiency of the method to more than few tens of nm s^{-1}. Moreover, the effects of atomic interactions were extensively assessed and contrasted to the ideal collision-less case making this study valuable for the non-condensed regime as well. The method proposed is not bound to a particular experimental arrangement and covers a wide range of fountain baselines from few mm to several meter-tall chambers without suffering from any performance deterioration. In general, the acceleration ramps can be engineered to account for an initial spatial offset between the two atomic clouds, which was for simplicity omitted in the treated example. This feature is an intrinsic advantage of the scheme that provides a solution to the gravitational sag issue complicating Earth-bound inertial precision measurements. The choice of the atomic test pair is not restricted to the study case considered but can be made among the multitude of alkaline and alkaline-Earth-metal species possessing tune-out wavelengths [32–42, 50]. The fountain concept presented is the baseline of a launch stage in an atomic interferometry test of the equivalence principle requiring the two species to start with velocities as close as few nm s^{-1}. This result puts a WEP test with an uncertainty of 10^{-15} within reach in already existing fountain facilities.

Acknowledgments

RC thanks the German Academic Exchange Service (DAAD) for funding research stays during this study. HA, CS, EMR and NG thank the DFG collaborative research centre (SFB) 'geo-Q' and acknowledge the support of the German Space Agency (DLR) with funds provided by the Federal Ministry of Economic affairs and Energy (BMWi) due to an enactment of the German Bundestag under Grant No. DLR 50WM1131-1137 (project QUANTUS-III). NG would like to thank Jason Hogan and Jan Rudolph for stimulating discussions.

References

[1] Grimm R, Weidemüller M and Ovchinnikov Y B 2000 Optical dipole traps for neutral atoms *Adv. At. Mol. Opt. Phys.* **42** 95
[2] Ketterle W 2002 Nobel lecture: When atoms behave as waves: Bose–Einstein condensation and the atom laser *Rev. Mod. Phys.* **74** 1131
[3] Cornell E A and Wieman C E 2002 Nobel lecture: Bose–Einstein condensation in a dilute gas, the first 70 years and some recent experiments *Rev. Mod. Phys.* **74** 875
[4] Bloch I 2005 Ultracold quantum gases in optical lattices *Nat. Phys.* **1** 23
[5] Ben Dahan M *et al* 1996 Bloch oscillations of atoms in an optical potential *Phys. Rev. Lett.* **76** 4508
[6] Wilkinson S R *et al* 1996 Observation of atomic Wannier–Stark ladders in an accelerating optical potential *Phys. Rev. Lett.* **76** 4512
[7] Battesti R *et al* 2004 Bloch oscillations of ultracold atoms: a tool for a metrological determination of h/m_{rb} *Phys. Rev. Lett.* **92** 253001
[8] Müller H *et al* 2009 Atom interferometers with scalable enclosed area *Phys. Rev. Lett.* **102** 240403
[9] Bouchendira R *et al* 2011 New determination of the fine structure constant and test of the quantum electrodynamics *Phys. Rev. Lett.* **106** 080801
[10] Dickerson S M *et al* 2013 Multiaxis inertial sensing with long-time point source atom interferometry *Phys. Rev. Lett.* **111** 083001
[11] McDonald G D *et al* 2014 A faster scaling in acceleration-sensitive atom interferometers *Europhys. Lett.* **105** 63001
[12] McDonald G D *et al* 2013 80$\hbar k$ momentum separation with Bloch oscillations in an optically guided atom interferometer *Phys. Rev.* A **88** 053620
[13] Peters A, Chung K Y and Chu S 1999 Measurement of gravitational acceleration by dropping atoms *Nature* **400** 849
[14] Duan X-C *et al* 2014 Operating an atom-interferometry-based gravity gradiometer by the dual-fringe-locking method *Phys. Rev.* A **90** 023617
[15] Gillot P *et al* 2014 Stability comparison of two absolute gravimeters: optical versus atomic interferometers *Metrologia* **51** L15
[16] Hauth M *et al* 2013 First gravity measurements using the mobile atom interferometer gain *Appl. Phys.* B **113** 49
[17] Altin P A *et al* 2013 Precision atomic gravimeter based on bragg diffraction *New J. Phys.* **15** 023009
[18] Viola L and Onofrio R 1997 Testing the equivalence principle through freely falling quantum objects *Phys. Rev.* D **55** 455
[19] Will C M 2014 The confrontation between general relativity and experiment *Living Rev. Relativ.* **17** 4
[20] Fray S *et al* 2004 Atomic interferometer with amplitude gratings of light and its applications to atom based tests of the equivalence principle *Phys. Rev. Lett.* **93** 240404
[21] Bonnin A *et al* 2013 Simultaneous dual-species matter-wave accelerometer *Phys. Rev.* A **88** 043615
[22] Schlippert D *et al* 2014 Quantum test of the universality of free fall *Phys. Rev. Lett.* **112** 203002
[23] Tarallo G *et al* 2014 Test of einstein equivalence principle for 0-spin and half-integer-spin atoms: search for spin-gravity coupling effects *Phys. Rev. Lett.* **113** 023005
[24] Dimopoulos S *et al* 2007 Testing general relativity with atom interferometry *Phys. Rev. Lett.* **98** 111102
[25] Zhou L *et al* 2011 Development of an atom gravimeter and status of the 10 m atom interferometer for precision gravity measurement *Gen. Relativ. Gravit.* **43** 1931
[26] Hartwig J *et al* 2015 Testing the universality of free fall with rubidium and ytterbium in a very large baseline atom interferometer *New J. Phys.* **17** 035011
[27] Hogan J M, Johnson D M S and Kasevich M A 2009 Light-pulse atom interferometry *Optics and Space Physics* ed E Arimondo *et al* (Amsterdam: IOS) p 411
[28] Barrett B *et al* 2015 Correlative methods for dual-species quantum tests *New. J. Phys.* **17** 085010
[29] Dubetsky B and Kasevich M A 2006 Atom interferometer as a selective sensor of rotation or gravity *Phys. Rev.* A **74** 023615
[30] Bertoldi A 2010 Flattening Earth acceleration in atomic fountains *Phys. Rev.* A **82** 013622
[31] McGuirk J M *et al* 2002 Sensitive absolute-gravity gradiometry using atom interferometry *Phys. Rev.* A **65** 033608
[32] LeBlanc L J and Thywissen J H 2007 Species-specific optical lattices *Phys. Rev.* A **75** 053612

[33] Arora B, Safronova M S and Clark C W 2011 Tune-out wavelengths of alkali-metal atoms and their applications *Phys. Rev.* A **84** 043401
[34] Topcu T and Derevianko A 2013 Tune-out wavelengths and landscape-modulated polarizabilities of alkali-metal rydberg atoms in infrared optical lattices *Phys. Rev.* A **88** 053406
[35] Cheng Y, Jiang J and Mitroy J 2013 Tune-out wavelengths for the alkaline-Earth-metal atoms *Phys. Rev.* A **88** 022511
[36] Mitroy J and Tang L-Y 2013 Tune-out wavelengths for metastable helium *Phys. Rev.* A **88** 052515
[37] Jiang J, Tang L-Y and Mitroy J 2013 Tune-out wavelengths for potassium *Phys. Rev.* A **87** 032518
[38] Safronova M S, Safronova U I and Clark C W 2012 Magic wavelengths for optical cooling and trapping of lithium *Phys. Rev.* A **86** 042505
[39] Safronova M S, Safronova U I and Clark C W 2013 Magic wavelengths for optical cooling and trapping of potassium *Phys. Rev.* A **87** 052504
[40] Thalhammer G *et al* 2008 Double species Bose–Einstein condensate with tunable interspecies interactions *Phys. Rev. Lett.* **100** 210402
[41] Gadway B *et al* 2012 Probing an ultracold-atom crystal with matter waves *Nat. Phys.* **8** 544
[42] Trubko R *et al* 2015 Atom interferometer gyroscope with spin-dependent phase shifts induced by light near a tune-out wavelength *Phys. Rev. Lett.* **114** 140404
[43] Steck, Cesium d line data,1998 (http://steck.us/alkalidata/cesiumnumbers.pdf)
[44] Steck, Rubidium 85 d line data, 2008 (http://steck.us/alkalidata/rubidium85numbers.pdf)
[45] Steck, Rubidium 87 d line data, 2001 (http://steck.us/alkalidata/rubidium87numbers.pdf)
[46] Tiecke, Properties of potassium, 2010 (http://tobiastiecke.nl/archive/PotassiumProperties.pdf)
[47] Steck, Sodium d line data, 2000 (http://steck.us/alkalidata/sodiumnumbers.pdf)
[48] Gehm, Properties of ^{6}li, 1998 (http://physics.ncsu.edu/jet/techdocs/pdf/PropertiesOfLi.pdf)
[49] Herold C D *et al* 2012 Precision measurement of transition matrix elements via light shift cancellation *Phys. Rev. Lett.* **109** 243003
[50] Holmgren W F *et al* 2012 Measurement of a wavelength of light for which the energy shift for an atom vanishes *Phys. Rev. Lett.* **109** 243004
[51] Catani J *et al* 2009 Entropy exchange in a mixture of ultracold atoms *Phys. Rev. Lett.* **103** 140401
[52] Kishimoto T *et al* 2009 Direct evaporative cooling of ^{41}Køpenup into a Bose–Einstein condensate *Phys. Rev.* A **79** 031602
[53] Modugno G *et al* 2001 Bose–Einstein condensation of potassium atoms by sympathetic cooling *Science* **294** 1320
[54] Hu Z-K *et al* 2011 Simultaneous differential measurement of a magnetic-field gradient by atom interferometry using double fountains *Phys. Rev.* A **84** 013620
[55] Pethick C J and Smith H 2001 *Bose–Einstein Condensation in Dilute Gases* (Cambridge: Cambridge University Press)
[56] Pötting S *et al* 2001 Coherent acceleration of Bose–Einstein condensates *Phys. Rev.* A **64** 023604
[57] Rosen G 1972 Galilean invariance and the general covariance of nonrelativistic laws *Am. J. Phys.* **40** 683
[58] Colella R, Overhauser A W and Werner S A 1975 Observation of gravitationally induced quantum interference *Phys. Rev. Lett.* **34** 1472
[59] Greenberger D M 1979 Some remarks on the extended galilean transformation *Am. J. Phys.* **47** 35
[60] Fleck J A, Morris J R and Feit M D 1976 Time-dependent propagation of high energy laser beams through the atmosphere *Appl. Phys.* **10** 129
[61] Gaaloul N *et al* 2006 Theoretical study of a cold-atom beam splitter *Phys. Rev.* A **74** 023620
[62] Jaouadi A *et al* 2010 Bose–Einstein condensation in dark power-law laser traps *Phys. Rev.* A **82** 023613
[63] Rahman R 2011 The intel math kernel library and its fast Fourier transform routines (https://software.intel.com/en-us/articles/the-intel-math-kernel-library-and-its-fourier-transform-routines)
[64] Kosloff R and Tal-Ezer H 1986 A direct relaxation method for calculating eigenfunctions and eigenvalues of the Schrödinger equation on a grid *Chem. Phys. Lett.* **127** 223
[65] Adhikari S K 2003 Expansion of a Bose–Einstein condensate formed on a joint harmonic and one-dimensional optical-lattice potential *J. Phys. B: At. Mol. Opt. Phys.* **36** 3951
[66] Morsch O *et al* 2002 Free expansion of a Bose–Einstein condensate in a one-dimensional optical lattice *Phys. Rev.* A **66** 021601
[67] Gustavsson M *et al* 2008 Control of interaction-induced dephasing of Bloch oscillations *Phys. Rev. Lett.* **100** 080404
[68] Witthaut D *et al* 2005 Bloch oscillations of Bose–Einstein condensates: breakdown and revival *Phys. Rev.* E **71** 036625
[69] Kovachy T *et al* 2015 Matter wave lensing to picokelvin temperatures *Phys. Rev. Lett.* **114** 143004
[70] Szigeti S S *et al* 2012 Why momentum width matters for atom interferometry with Bragg pulses *New J. Phys.* **14** 023009
[71] Chu S *et al* 1986 Proposal for optically cooling atoms to temperatures of the order of 10^{-6} K *Opt. Lett.* **11** 73
[72] Ammann H and Christensen N 1997 Delta kick cooling: a new method for cooling atoms *Phys. Rev. Lett.* **78** 2088
[73] Müntinga H *et al* 2013 Interferometry with Bose–Einstein condensates in microgravity *Phys. Rev. Lett.* **110** 093602
[74] Aguilera D N *et al* 2014 Ste-quest test of the universality of free fall using cold atom interferometry *Class. Quantum Grav.* **31** 115010